

Early detection of drought stress in grass swards with imaging spectroscopy

A.G.T. Schut* and J.J.M.H. Ketelaars

Plant Research International, Wageningen University and Research Centre, P.O. Box 16, NL-6700 AA Wageningen, The Netherlands

* Corresponding author (tel: +31-317-475939; fax: +31-317-423110; e-mail: tom.schut@wur.nl)

Received 17 December 2002; accepted 25 August 2003

Abstract

The potential of an experimental imaging spectroscopy system with high spatial (0.28–1.45 mm²) and spectral (5–13 nm) resolution was explored for early detection of drought stress in grass. A climate chamber experiment was conducted with nine *Lolium perenne* L. mini swards with drought stress treatments at two nitrogen levels. Images were recorded once every two days. Growth was monitored by changes in ground cover (GC), index of reflection intensity (IRI) and wavelength position of and gradient at inflection points, as estimated from images. Drought stress increased leaf dry matter and sugar content. Drought stress decelerated and ultimately reversed GC evolution, and kept IRI at low values. In contrast to unstressed growth, all absorption features narrowed and became shallower under drought stress. The inflection points near 1390 and 1500 nm were most sensitive to drought stress. Differences between drought stress and control swards were detected shortly before leaf water content dropped below 80%. The evolution of inflection point wavelength positions reversed under drought stress, except for the inflection point at the red edge where the shift to longer wavelengths during growth accelerated. The relation between inflection points at 705 and 1390 nm differentiated unstressed swards at an early growth stage from drought-stressed swards in a later growth stage.

Additional keywords: imaging spectrometry, hyperspectral, grassland, leaf reflectance

Introduction

Water resources for agriculture are limited, urging optimization of irrigation water use. Irrigation optimization strategies include temporal and spatial differentiation. In grassland, duration and intensity of drought stress influence tiller survival (Grashoff *et al.*, 2001). Therefore, an accurate timing of irrigation may prevent sward deterioration. In grass swards under drought stress first growth rate decreases and in more advanced stages of drought stress morphological changes and eventually leaf senescence and

leaf death take place (Jones & Lazenby, 1988). With accurate drought stress detecting sensors, new irrigation management tools can be developed, limiting irrigation water use and preventing long-term production loss.

Dehydration of leaves decreases light absorption by water and severe dehydration affects pigment light-absorption. Dehydration also changes internal leaf structure. However, changes in internal leaf structure are less important than effects of pigment and water absorption for reflection and absorption characteristics of stressed leaves (Carter, 1991). So if water is lost, reflectance of leaves increases in both visible and infrared wavelengths (Ripple, 1986; Bowman, 1989; Inoue *et al.*, 1993; Penuelas & Inoue, 1999). For passive sensors only wavelengths with abundant natural light can be used for stress detection, eliminating the use of strong water absorption bands. Remote sensing of drought stress in crops is further complicated by changes in leaf area index (LAI) and ground cover, canopy geometry, fraction of dead leaf material and background soil reflectance (Jackson & Ezra, 1985; Ripple, 1986; Hunt *et al.*, 1987; Penuelas *et al.*, 1993; Fernández *et al.*, 1994).

With a recently developed imaging spectroscopy system new and automatic means for grass sward characterization have become available (Schut *et al.*, 2002). Reflection intensity measured with this system is related to leaf height in the canopy and leaf angle. With reflection intensity, image ground cover (GC)¹ can be differentiated into reflection intensity classes where the pixel distribution over intensity classes relates to canopy geometry (Schut *et al.*, 2002). The non-destructive nature of reflection measurements allows the study of the evolution of GC, canopy geometry and leaf pixel spectra. From GC data light interception, LAI and biomass can be estimated (Schut & Ketelaars, 2003a). Sward heterogeneity can be quantified with spatial GC variability and is related to production capacity (Schut & Ketelaars, 2003b).

In this paper the potential of this experimental system is explored for early detection of drought stress in grass swards. For this purpose a climate chamber experiment was conducted with 9 *Lolium perenne* L. mini swards from 1 through 27 November 2000. Evolution of GC, spatial GC variability and spectral characteristics in response to drought stress were studied. To this end, images of drought-stressed swards with low and high nitrogen (N) supply were recorded throughout one growth period, and shifts of and gradients near inflection points were studied with derivative spectra.

Materials and methods

Experiment

From 1 to 27 November 2000, 9 mini swards of *Lolium perenne* L. were grown under abundant light (16 hours under HPI 400[®] light source (120 W m⁻²) and 8 hours dark). Temperatures were kept at 20 °C during the day and at 15 °C during the night, with 65% relative humidity during the day and 80% during the night. Swards were grown in containers (0.9 m long, 0.7 m wide, 0.4 m high). The mini-sward containers were

¹ For abbreviations used see Appendix.

taken from a N experiment (Schut & Ketelaars, 2003c). Only containers with mini-swards were used that previously had received adequate N nutrition (60, 90 or 120 kg N ha⁻¹ per harvest in the growing season). The containers were evenly distributed over the treatments: control with high N supply (Co), drought-stressed with high N supply (DS-HN) and drought-stressed with low N supply (DS-LN), with three replicates per treatment. There were not enough mini-swards available to include a control with low N supply. At the start of the experiment the low N and high N treatments were fertilized with 30 and 120 kg N ha⁻¹, respectively.

The mini-swards started with 20% (volume) soil moisture. During the experiment no extra water was supplied to the DS-LN and DS-HN mini-swards. The Co mini-swards were kept at 20% soil moisture, with water supplied through perforated tubes. To minimize changes in canopy geometry these tubes were placed under the canopy on top of the soil. Once every two days the containers were weighed. Leaf dry matter (DM) content was measured to monitor the degree of drought stress. For this purpose, 10 top canopy leaves were sampled per mini-sward and dried (105 °C) overnight for DM content determination.

Chemical analyses

At harvest (27 November), fresh matter yield was weighed and samples were taken for analysis of dry matter, total N, nitrate and sugar content. Total N was determined on a Vario EL® (Elementar Analyse Systemen, GmbH Hanau), and nitrate on a TRAACS 800® continuous flow system (Bran and Luebbe Inc., Roselle, USA). Sugars were determined in dried material. The sugars were extracted by adding demineralized water to a ground sample. On a Bran and Luebbe AutoAnalyzerII (Bran and Luebbe Inc., Roselle, USA, Method NL213-89FT), the content of reducing sugars (glucose and fructose) was measured by reaction with ferricyanide, which is reduced to colourless ferrocyanide. The reduction in light absorbance at 420 nm was used to calculate the content of sugars as glucose equivalents. Total sugars after hydrolysis were determined in the same extract but the autoanalyzer was now equipped with a hydrolysis-step to convert di- and oligo-saccharides to glucose and fructose.

Images

Image recording

At 42 positions in each mini-sward, image lines were recorded once every two days. At each position reflection was measured with three sensors (V7, N10 and N17), in the wavelength ranges 404–709 nm (V7), 680–970 nm (N10) and 960–1650 (N17); for details see Schut *et al.* (2002). At soil level, an image line recorded by the V7 and N10 was 1.39 mm wide and 152.5 mm long. For the N17 sensor, an image line was 1.39 mm wide and 133.1 mm long. There were 768 (V7 and N10) and 128 (N17) pixels per image line for the spatial dimension, resulting in a spatial resolution of 0.28 mm² and 1.45 mm² per pixel, respectively. Per pixel, radiance was measured in 565 (V7 and N10) and 128 (N17) spectral bands. The spectral resolution was 5 nm for the V7 and N10 sensor and 13 nm for the N17 sensor. The system used xenon and halogen light sources with

lenses that only illuminated the area (2–4 cm wide strip) where an image line was recorded. Light was projected vertically to the soil, and reflection was measured under an angle of 2 degrees from nadir, minimizing shadow effects. Per sensor the imaging spectroscopy system recorded a single image line with the light sources switched off and 5 image lines from a 50% reflection standard as part of the sampling routine. With these standard image lines, reflectance was calculated from the radiance data.

Classification

Schut *et al.* (2002) defined threshold values for soil, grass leaves, leaves with specular reflection, dead material classes and for an intermediate class between soil and dead material. Separation between classes was based on ratios of reflectance at 450, 550 and 680 nm. These classes were subdivided into reflection intensity classes (IC), based on the reflection intensity at predefined wavelengths (550 nm for the V7, 746 nm for the N10 and 1100 nm for the N17 sensor). For grass the intensity classes ranged from IC 0 up to and including IC 6 for the V7 sensor and from IC 0 up to and including IC 10 for the N10 and N17 sensors. For leaves with specular reflection, IC ranged from 0 up to and including 2, and for dead material from IC 0 up to and including 3. A large number of pixel reflection spectra per intensity class is available in a spectral library. With this library, pixel spectra of the recorded image lines were classified with maximum likelihood procedures (Schut & Ketelaars, 2003a). The classification procedure was based on a limited number of selected wavelengths, maximizing class to class separation (Feyaerts & Van Gool, 2001).

After classification, spectra of pixels were normalized according to equations in Schut *et al.* (2002). Normalization means that reflection was divided by the mean reflection in the 550–555 nm range for the V7 sensor, in the 800–850 nm range for the N10 sensor and in the 1070–1130 nm range for the N17 sensor. Mean sward reflection spectra (MSS) were calculated from normalized spectra of all pixels in grass IC 1 through 10. In addition, mean reflection spectra were calculated from normalized spectra for each IC (MICS). It is emphasized that for this procedure only grass pixels were selected, eliminating pixels containing soil and dead material. Assuming that the data of the V7 sensor and the N10 sensor were from identical objects and that the sensitivity of the sensors in overlapping regions was comparable, the data of the V7 sensor were normalized to the 800–850 nm range (Schut *et al.*, 2002). These assumptions seem valid for MSS as the reflection of leaves are measured with both sensors on similar positions in the sward.

Ground cover, index of reflection intensity and spatial heterogeneity of ground cover

Ground cover (GC) was calculated per mini-sward for each intensity class (IC). Total image line (IL) ground cover (GC_{IL} , %) was calculated as percentage area coverage of all grass IC (GCG) and IC of all specular classes (GCS) from the V7 sensor using the formula:

$$GC_{IL} = \sum_{ic=0}^6 GCG_{ic} + \sum_{ic=0}^2 GCS_{ic}$$

where

ic = the index number of the intensity class, and

N = the total number of pixels per image line.

The mini-sward GC was calculated as the average of the GC_{IL} over the 42 image lines. This mini-sward GC estimate underestimates visually scored GC, which is equal to $8.63 + 1.076 \times GC$ (Schut *et al.*, 2002). The index of reflection intensity (IRI, %) was then calculated with the formula:

$$IRI = 100 \times \frac{\sum_{ic=3}^6 \frac{I}{42} \sum_{IL=1}^{42} GCG_{IL,ic}}{GC}$$

IRI measures the presence of highly reflecting green pixels as a percentage of GC. A high value represents a dense canopy with horizontally oriented leaves (Schut & Ketelaars, 2003a).

The spatial heterogeneity was quantified with the spatial standard deviation of GC (GC-SSD) and logistically transformed values of GC (TGC-SSD), which were calculated according to Schut & Ketelaars (2003b):

$$TGC_{IL} = \ln \left(\frac{GC_{IL}}{101 - GC_{IL}} \right)$$

The spatial standard deviation was calculated per mini-sward as the standard deviation of the 42 GC_{IL} or TGC_{IL} estimates.

Calculation of chlorophyll-dominated absorption width

Reflectance spectra of green material typically have a sharp transition from minimum reflection around 680 nm and maximum reflection around 750 nm, known as the red edge (RE) (Horler *et al.*, 1983). Green material reflects more radiation in the green part than in the blue or red parts of the spectrum, and a blue edge (BE) and a green edge (GE) can be found around 520 and 600 nm. In earlier work, Schut & Ketelaars (2003c) used a chlorophyll-dominated absorption width (CAW) measure between the half height of the green and red edge. This measure was strongly related to relative growth deficit due to N shortage.

Calculation of derivative spectra

The mean sward reflection spectra (MSS) were smoothed with cubic splines. Splines are non-parametric regression functions, mostly third order polynomials, where a regression curve is calculated for each interval between knots. The regression curve is continuous between intervals at the first and second derivative (Silverman, 1985). The number of knots was arbitrarily set to one third of the number of spectral bands. Decreasing the number of knots smoothes the spectral curve more strongly, removing small features. The effects of the choice of the number of knots on the selected

features were evaluated by setting the number of knots to one ninth of the number of spectral bands. First and second derivatives were determined from the resulting curves. The minimum or maximum derivative wavelength was defined as the point of intersection of the second derivative with the abscissa (Railyan & Korobov, 1993). These points of intersection will be referred to as inflection points (IP, nm). The gradient values at the IPs, calculated as Δ reflection per Δ nm over the two nearest bands, were also determined. The gradients and IP only slightly changed with the choice of number of knots. Therefore, the values of the IP and gradients presented were calculated with the number of knots set to one third of the number of spectral bands.

Statistics

The statistical differences were evaluated with analysis of variance. The null hypothesis was that treatment means on the same date did not differ. This hypothesis was tested with a two-sided t-test ($P < 0.05$).

Results

Dry matter yield and chemical analyses

Dry matter (DM) yield of the drought-stressed treatments was significantly lower than of the control (Table 1). Drought stress affected all variables but only nitrate of DS-HN and control were not statistically significantly different. Drought stress increased DM, reducing sugar and total sugar content. Total sugar content increased from 14.7% for Co to 23.8% for DS-HN and to 25.5% for DS-LN. The DS-LN had lower N and nitrate contents than DS-HN and Co. The N content was slightly lower for DS-HN than for Co, but there was no statistical difference in nitrate content (Table 1).

Table 1. Means with standard deviations of dry matter (DM) yield and contents of DM, reducing sugars, total sugars, N and nitrate for control and drought-stressed swards with high (DS-HN) and low (DS-LN) N supply.

	Sward		
	Control	DS-HN	DS-LN
DM yield (kg DM ha ⁻¹)	2000 ± 108a ¹	761 ± 276b	649 ± 122b
DM (%)	16.93 ± 0.8a	39.13 ± 7.3b	34.37 ± 2.9b
Reducing sugars (%)	3.22 ± 0.26a	4.39 ± 0.55b	4.50 ± 0.26b
Total sugars (%)	14.7 ± 1.8a	23.8 ± 3.5b	25.5 ± 1.3b
N (%)	3.81 ± 0.09a	3.40 ± 0.20b	2.26 ± 0.17c
Nitrate (%)	0.51 ± 0.05a	0.51 ± 0.04a	0.04 ± 0.01b

¹ Means in the same row, followed by a different letter are statistically different ($P < 0.05$).

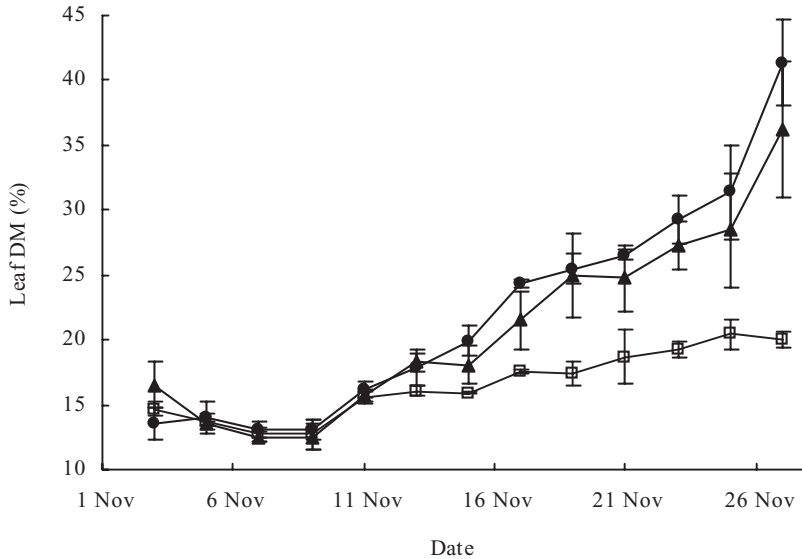


Figure 1. Development of leaf dry matter content for control swards (□), drought-stressed swards with high N supply (●) and drought-stressed swards with low N supply (▲). Error bars indicate standard error of means.

During growth, leaf DM content of Co increased but did not exceed 21% (Figure 1). From 13 November onwards, DM contents of DS-HN and DS-LN were higher than DM content of Co. DM content of DS-HN differed significantly from Co for the first time on 13 November and DS-LN differed significantly from Co for the first time on 17 November. Soil moisture content of DS-HN dropped below 11% two days earlier than DS-LN, and DM content for DS-HN also responded slightly earlier than for DS-LN (Figure 1).

Image analysis

Ground cover, index of reflection intensity and spatial standard deviation of ground cover Ground cover (GC) of Co increased steadily up to 27 November (Figure 2). DS-LN had a slightly higher initial GC. Growth rates of GC of DS-HN and DS-LN decreased after 9 November and became negative after 17 November, resulting in a decrease in GC due to folding and eventually dying of leaves. From 15 November onwards error bars of drought-stressed treatments are longer, indicating that differences between replicates of drought-stressed swards increased. The index of reflection intensity (IRI) of Co increased strongly after 17 November, whereas the IRI of DS-HN and DS-LN remained constant (Figure 3). Drought stress visibly changed leaf angle to a more horizontal orientation, but also decreased mean leaf height. Due to these two opposite effects IRI values increased only slightly.

The GC-SSD of Co remained below 11% (volume) during all intervals, whereas the

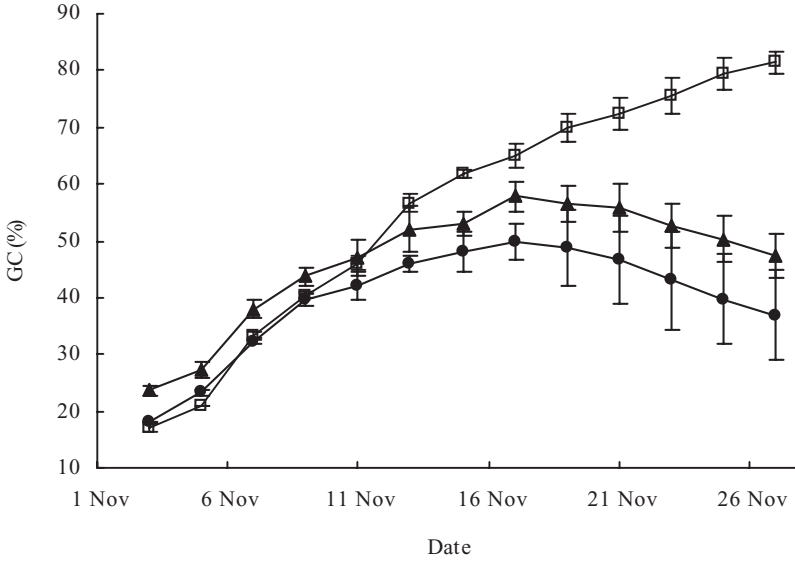


Figure 2. Development of image ground cover (GC) for control swards (□), drought-stressed swards with high N supply (●) and drought-stressed swards with low N supply (▲). Error bars indicate standard error of means.

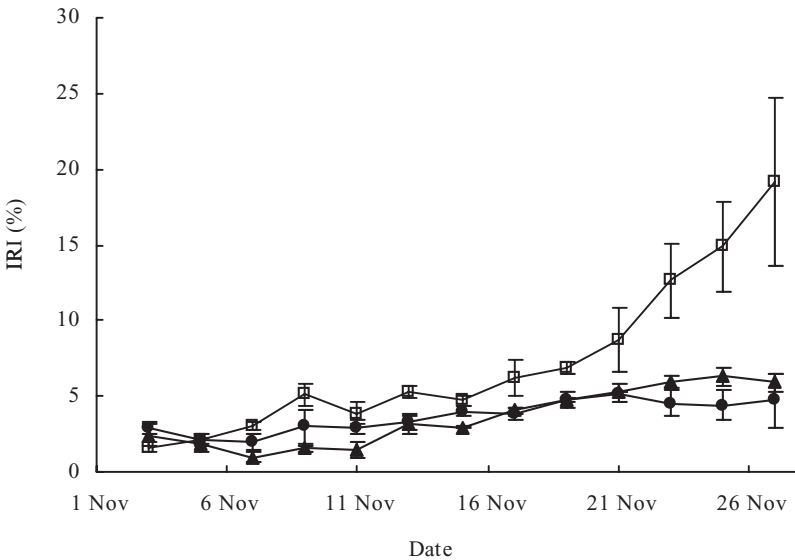


Figure 3. Development of index of reflection intensity (IRI) for control swards (□), drought-stressed swards with high N supply (●) and drought-stressed swards with low N supply (▲). Error bars indicate standard error of means.

Table 2. Spatial standard deviation of ground cover (GC-SSD, %) and logistically transformed ground cover (TGC-SSD, -/-) with standard error of replicate mean for intervals of growth days for control and drought-stressed swards with high (DS-HN) and low (DS-LN) N supply.

Growth days	Sward		
	Control	DS-LN	DS-HN
<i>GC-SSD</i>			
1-4	8.1 ± 0.9a [†]	8.6 ± 0.8a	8.1 ± 0.1a
5-8	9.3 ± 0.6a	10.0 ± 0.5a	10.7 ± 0.4a
9-13	11.0 ± 0.6ab	10.3 ± 0.3a	12.3 ± 0.4b
14-21	9.1 ± 0.7a	10.8 ± 1.1a	11.8 ± 1.1a
27	6.5 ± 0.8a	11.0 ± 1.8b	12.8 ± 0.8b
<i>TGC-SSD</i>			
1-4	0.57 ± 0.04a	0.51 ± 0.03a	0.53 ± 0.02a
5-8	0.51 ± 0.05a	0.47 ± 0.03a	0.56 ± 0.01a
9-13	0.47 ± 0.03ab	0.43 ± 0.01a	0.53 ± 0.02b
14-21	0.46 ± 0.03a	0.47 ± 0.04a	0.51 ± 0.06a
27	0.47 ± 0.06a	0.47 ± 0.09a	0.66 ± 0.09a

[†] Means in the same row, followed by a different letter are statistically different ($P < 0.05$).

GC-SSD first increased and then decreased (Table 2). The GC-SSD values of DS-LN and DS-HN remained constant from 13 days after harvest. Therefore, the statistically significant differences in GC-SSD between DS-LN and DS-HN and Co just before harvest (27 days of growth) mainly resulted from differences in GC evolution. The TGC-SSD remained below 0.6 for all intervals and treatments, except for DS-HN at 27 growth days with a value of 0.66. Only one of the three DS-HN containers showed a strong TGC-SSD increase towards harvest. This indicates that the GC decrease was not evenly distributed over this container. The differences between the drought-stressed swards and Co were not statistically significant.

Derivative spectra

The drought-stressed swards had a higher reflection than Co in the visible wavelength range and in the range above 1100 nm, whereas reflection was lower in the 730–830 nm range (Figure 4A). The amplitude of the derivatives of DS-HN and DS-LN was lower than that of Co throughout the spectral range measured. The dots in Figure 4B indicate that 17 IPs were identified (at 463, 480, 485, 519, 570, 595, 608, 624, 640, 705, 768, 960, 990, 1140, 1220, 1390 and 1510 nm). The IPs at 519, 570, 705, 990, 1140, 1390 and 1510 nm corresponded to clearly visible slopes (Figure 4) that were also selected with the number of knots set to one ninth of the number of spectral bands. The IPs at 463, 480, 485, 595, 608, 624 and 640 nm corresponded to less strong absorption features, but these features were present in spectra of all data.

During unstressed growth, absorption features became deeper and wider, resulting in IP shifts. Under drought stress, water absorption features became narrower, resulting in reversed IP shifts. Table 3 presents the pigments and chemical bonds with light-absorbing or emitting features near the IP and the evolution of IPs with statistically

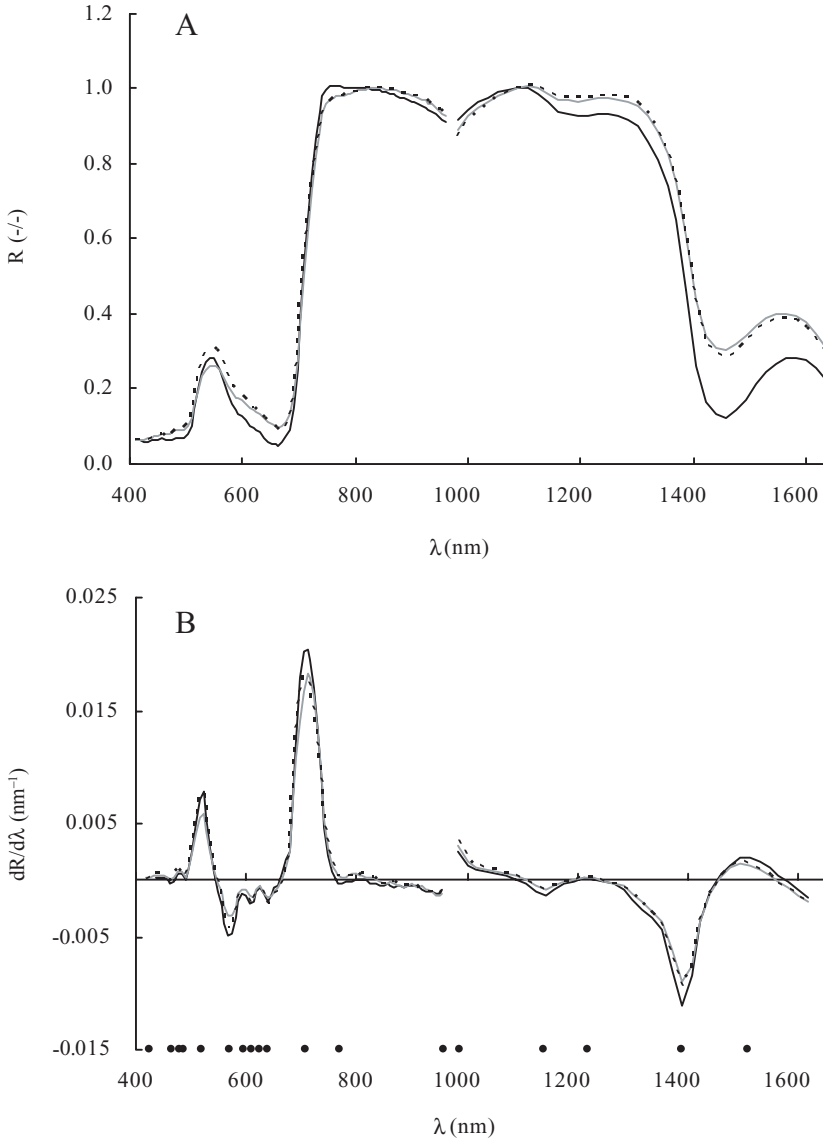


Figure 4. Normalized reflection (R) curve (A) and first derivative (B) for control (—), DS-HN (---) and DS-LN (· · ·) swards on 23 November. Dots indicate wavelengths of selected minima and maxima of the first derivative.

Table 3. Mean inflection points (IP, nm) for control (Co) and drought-stressed swards with high (DS-HN) and low (DS-LN) N supply during the period 3–27 November. The indicated pigments [β -carotene (Car), chlorophyll a (Chla) and b (Chlb)] and chemical bonds have an absorption or emission maximum near IPs (after Curran, 1989; Lichtenthaler, 1987; Zarco Tejada *et al.*, 2000).

Sward	Pigment or bond	Date						
		3/11	9/11	11/11	13/11	17/11	23/11	27/11
Co	Chlb+Car	481.2a ¹	479.3a	479.2a	479.0a	478.3a	480.2a	479.7a
DS-LN	Chlb+Car	480.0a	478.9a	478.1a	479.2a	479.7b	479.4ab	478.1a
DS-HN	Chlb+Car	480.2a	478.6a	478.1a	478.6a	479.3ab	478.7b	478.6a
Co	Car	484.2a	485.6a	486.4ab	486.7a	486.5a	486.4a	485.5a
DS-LN	Car	484.9a	486.6a	486.6a	487.4a	487.2a	486.7a	487.7ab
DS-HN	Car	485.5a	485.9a	485.6b	487.3a	488.2a	488.3b	489.2b
Co	Car+Chlb	516.4a	518.4a	519.1a	519.1a	519.6a	519.6a	519.6a
DS-LN	Car+Chlb	516.7a	518.8b	519.2a	519.2a	519.2b	519.4a	519.7a
DS-HN	Car+Chlb	516.5a	518.6c	519a	519.2a	519.5a	519.5a	519.4a
Co	Chlb	571.9a	569.5a	569.5a	569.3a	569.1a	569.1a	569.2a
DS-LN	Chlb	571.2a	569.8a	569.5a	569.5a	569.8a	570.1b	570.4b
DS-HN	Chlb	572.0a	570.0a	569.6a	569.5a	569.8a	570.2b	571.1b
Co	Chla	622.8a	625.0a	625.2a	624.5a	625.4a	625.1a	624.4a
DS-LN	Chla	622.6a	624.9a	624.9a	625.2a	624.7ab	623.7ab	623.9ab
DS-HN	Chla	622.5a	624.6a	624.1a	624.9a	623.4b	623.4b	622.0b
Co	Chlb	639.3a	640.8a	640.9a	639.4a	639.5a	639.6a	638.9a
DS-LN	Chlb	640.7a	640.9a	639.4a	640.7a	640.3a	638.4a	640.2a
DS-HN	Chlb	641.5a	638.6a	638.1a	638.9a	637.7b	639.2a	638.9a
Co	Chla	696.2a	703.3a	706.5a	706.3a	706.9a	708.1ab	709.6ab
DS-LN	Chla	695.0a	705.9b	705.8a	707.8b	707.8a	707.0a	708.7a
DS-HN	Chla	694.9a	704.6ab	707.8a	708.5b	709.5a	710.6b	711.7b
Co	Fluoresc.	763.5a	765.8a	766.1a	767.0a	771.6a	770.5a	770.6a
DS-LN	Fluoresc.	763.5a	766.2a	766.9a	767.7a	770.9a	775.1a	776.3ab
DS-HN	Fluoresc.	762.4a	767.6a	765.8a	767.6a	771.1a	774.9a	781.6b
Co	O-H	962.6a	961.6a	961.1a	960.2a	959.6a	959.1a	957.6a
DS-LN	O-H	962.6a	962.0b	961.9a	961.4b	961.6b	962.0b	961.6b
DS-HN	O-H	962.6a	961.9ab	961.4a	961.2ab	961.4b	962.0b	961.4b
Co	O-H	996.6a	992.6a	992.0a	989.8a	987.6a	986.8a	981.9a
DS-LN	O-H	996.6a	994.1b	993.6a	992.3a	992.8b	993.5b	992.9b
DS-HN	O-H	996.6a	993.2a	992.6a	991.8a	992.4 b	993.7b	992.8b
Co	O-H	1142.9a	1139.2a	1139.3a	1139.4a	1138.6a	1137.9a	1138.4a
DS-LN	O-H	1139.7a	1139.6a	1140.1a	1139.4a	1140.5b	1141.1b	1144.1b
DS-HN	O-H	1142.4a	1139.2a	1138.7a	1139.5a	1141.1b	1142.4b	1143.3b
Co	O-H, C-H	1391.8a	1390.2a	1389.7a	1389.7a	1389.6a	1389.0a	1389.4a
DS-LN	O-H, C-H	1391.8a	1390.7a	1390.0a	1390.4b	1390.4b	1390.9b	1392.9b
DS-HN	O-H, C-H	1391.8a	1390.3a	1390.1a	1390.2b	1391.0c	1391.8b	1393.2b
Co	O-H, N-H	1499.8a	1500.3a	1504.7a	1504.5a	1506.4a	1508.0a	1506.6a
DS-LN	O-H, N-H	1499.0a	1499.1a	1501.0b	1502.9ab	1503.6b	1500.9b	1496.4b
DS-HN	O-H, N-H	1498.5a	1501.4a	1502.8ab	1502.0b	1502.6b	1499.7b	1497.0b

¹ Means in the same row, followed by a different letter are statistically different ($P < 0.05$).

significant effects of drought stress. On 17 November, all IPs detected with the N₁₇ sensor and the IP near 960 nm of the N₁₀ sensor responded to drought. The IPs near the strongest water absorption feature, i.e., around 1390 and 1500 nm, responded earliest to drought stress. The evolution of IPs of DS-HN and DS-LN at 1140, 1390 and 1500 nm reversed after 11 November under drought stress, whereas the IP positions near 960 and 990 nm remained stable.

Drought stress accelerated shifts of IPs around 485, 707 and 768 nm, whereas the IPs around 624 and 570 nm shifted in opposite direction after 17 November (Table 3). The IPs around 480, 640 and 519 nm did not change significantly under drought stress.

There were no statistical differences between DS-LN and DS-HN in IP position in the near infrared (NIR) region. The IPs around 485 nm shifted less far to shorter wavelengths for DS-LN than for DS-HN, and the IPs around 624 and 705 nm shifted less to longer wavelengths.

The slopes of nearly all IPs became steeper during unstressed growth (Table 4). Under drought stress, slopes became less steep for all IPs around water absorption features. In contrast to IP position, the gradient around 517 nm significantly differed between DS-HN and Co just before harvest. Under moderate drought stress, slopes became less steep for most IPs. The accelerated shift of the IP position near 707 nm towards longer wavelengths under drought stress coincided with a decreased slope gradient. The gradient near 767 nm became negative under unstressed growth, whereas under drought stress gradients remained positive. This can be understood if the differences in general gradients between 740 and 800 nm of drought-stressed and unstressed leaves are considered (Figure 4). In this range, unstressed leaves had a nearly flat reflection curve whereas drought-stressed leaves showed a slight increase in reflection with wavelength. The chlorophyll fluorescence feature in unstressed leaves has a distinct right shoulder, whereas this shoulder is flat for drought-stressed leaves and the IP is then shifted to the first maximum derivative thereafter.

The N supply affected gradients at the IPs around 485, 517, 570, 624 and 640 nm, whereas there were no statistically significant differences between the gradients at NIR IPs for DS-LN and DS-HN.

The IP position near 1390 nm of unstressed swards in an early growth stage (shortly after harvest) is similar to stressed swards later in the growth period. Therefore, a reference is required to separate between growth stages. The relation between the IP position near 705 and 1390 nm provided such a reference (Figure 5). The measurements at the beginning of a growth period are located at the left top, and points from measurements later in the growth period are located to the right of the relation. The slope of the relation between the 705 nm and 1390 nm IP position for low ($\lambda_{1390} = 1495 - 0.15 \lambda_{705}$; $R^2 = 0.78$, $n = 6$) and high N supply during unstressed growth differed significantly, where the slope was less negative at low (-0.15) than at high N supply (-0.20). The combination of IPs larger than 706 nm and 1390.2 nm identified drought-stressed swards.

Chlorophyll-dominated absorption width

Under severe drought stress, DS-LN and DS-HN had a lower chlorophyll-dominated

Table 4. Mean derivatives ($\times 10^3$, in Δ reflection per Δ nm) near the inflection points for control (Co), and drought-stressed swards with high (DS-HN) and low (DS-LN) N supply during the period 3–27 November.

Sward	Typical pos. (nm)	Date						
		3/11	9/11	11/11	13/11	17/11	23/11	27/11
Co	480	1.53a	0.88a	0.74a	0.77a	0.62a	0.56a	0.51a
DS-LN	480	1.50a	0.91a	0.81a	0.79a	0.84b	0.83b	1.00b
DS-HN	480	1.48a	0.84a	0.71a	0.77a	0.82ab	0.84b	1.01b
Co	485	1.41a	0.61a	0.38a	0.36a	0.21a	0.33a	0.31a
DS-LN	485	1.28a	0.47b	0.32a	0.30a	0.42b	0.50b	0.41a
DS-HN	485	1.12a	0.46b	0.40a	0.26a	0.25ab	0.28a	0.33a
Co	517	8.5a	8.81a	8.15a	8.19a	8.02a	7.69a	7.59a
DS-LN	517	8.26a	7.84b	8.03a	7.62b	7.70a	7.50a	6.97a
DS-HN	517	8.67a	8.48ab	7.57a	7.45b	6.80b	5.81b	5.08b
Co	570	-3.59a	-5.15a	-4.87a	-5.03a	-5.03a	-4.81a	-4.69a
DS-LN	570	-3.62a	-4.59b	-4.86a	-4.64b	-4.57a	-4.14ab	-3.61b
DS-HN	570	-3.80a	-5.07ab	-4.45a	-4.50b	-4.02b	-3.14b	-2.51c
Co	623	-1.05a	-1.37a	-1.30a	-1.31a	-1.29a	-1.23a	-1.18a
DS-LN	623	-1.08a	-1.14a	-1.22a	-1.19a	-1.20a	-1.07ab	-0.98a
DS-HN	623	-1.02a	-1.24a	-1.30a	-1.23a	-1.02a	-0.73b	-0.60b
Co	640	-2.36a	-2.52a	-2.24a	-2.21a	-2.11a	-1.99a	-1.98a
DS-LN	640	-2.28a	-2.23a	-2.16a	-2.13a	-2.01a	-1.93ab	-1.70a
DS-HN	640	-2.46a	-2.41a	-1.96a	-2.03a	-1.93a	-1.56b	-1.26b
Co	707	16.41a	20.30a	20.70a	20.63a	20.56a	20.40a	20.18a
DS-LN	707	16.51a	19.41b	20.32a	19.93a	19.26a	18.46b	17.43b
DS-HN	707	16.74a	20.12a	20.18a	19.99a	18.96a	18.04b	17.09b
Co	767	1.07a	0.14a	-0.19a	-0.09a	-0.22a	-0.27a	-0.27a
DS-LN	767	1.06a	0.30a	0.16b	0.06a	0.04a	0.19b	0.34b
DS-HN	767	0.98a	0.05a	-0.01ab	0.04a	-0.02a	0.28b	0.44b
Co	963	-23.29a	-13.11a	-10.13a	-7.13a	-4.71a	-3.37a	-1.51a
DS-LN	963	-23.17a	-14.59a	-13.43a	-10.80b	-11.32b	-12.56b	-11.26b
DS-HN	963	-22.65a	-14.06a	-11.63a	-10.35ab	-10.32b	-11.89b	-9.07b
Co	997	2.60a	2.58a	2.36a	2.35a	2.27a	1.96a	0.75a
DS-LN	997	2.59a	2.49a	2.38a	2.26a	2.25a	2.31b	2.14a
DS-HN	997	2.53a	2.58a	2.36a	2.37a	2.20a	2.1ab	1.84a
Co	1140	-0.26a	-0.93a	-0.98a	-1.08a	-1.26a	-1.43a	-1.47a
DS-LN	1140	-0.17a	-0.65b	-0.81a	-0.91b	-0.98b	-0.81b	-0.66b
DS-HN	1140	-0.23a	-0.79c	-0.93a	-0.92b	-0.88b	-0.78b	-0.63b
Co	1392	-7.69a	-10.39a	-10.64a	-10.62a	-10.74a	-10.92a	-10.22a
DS-LN	1392	-7.69a	-8.90b	-9.29b	-9.32b	-9.78ab	-9.25b	-7.56b
DS-HN	1392	-7.10a	-9.79ab	-9.77ab	-9.49b	-9.20b	-8.36b	-6.89b
Co	1500	1.30a	1.93a	1.89a	1.91a	1.97a	2.10a	2.13a
DS-LN	1500	1.55b	1.64b	1.60a	1.74b	1.69b	1.54b	1.32b
DS-HN	1500	1.23c	1.78ab	1.70a	1.68b	1.64b	1.34b	1.19b

¹ Means in the same row, followed by a different letter are statistically different ($P < 0.05$).

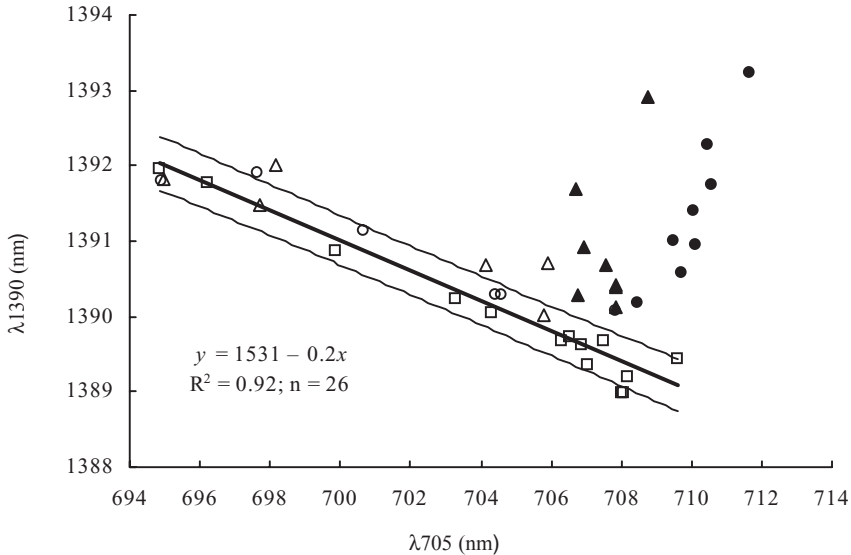


Figure 5. Relation between evolution of edges near 705 and 1390 nm. Open symbols indicate measurements of control (\square) and drought-stressed with high N (\circ) and low N supply (\triangle) before 12 November (no drought stress); closed symbols indicate measurements after 12 November (drought stress). The regression line is fitted through all points of the control. The thin lines indicate the 99% confidence interval for 1 new observation.

absorption width (CAW) than Co (Figure 6). CAW decreased when leaves started to shrink and GC decreased (Figure 2). Under drought stress, RE increased and GE decreased. This increase in RE is caused by a shift of the position of the first derivative maximum. The DM yield of DS-HN was 38.1% of Co, and of DS-LN 32.5% of Co with a CAW of 120.2 and 126.8 nm at harvest, respectively.

Discussion and conclusions

Drought stress increased leaf dry matter and sugar content, decelerated and ultimately reversed ground cover (GC) evolution and kept the index of reflection intensity (IRI) low. This GC development can be understood if it is considered that drought stress first decreases leaf photosynthesis and, in a more advanced stage of drought stress, specific leaf area (Jones *et al.*, 1980a, b). Thomas (1991) and Van Loo (1992) found that sugar content under drought stress strongly increased in *Lolium perenne* L. Drought stress became first visible in slower GC development. The GC estimates are linearly related to the light intercepting capacity of the sward. Reflection intensity measured with the system is related to leaf height in the canopy and leaf angle (Schut *et al.*, 2002). Therefore, IRI is a measure of canopy geometry and with the combination of GC and IRI, dry matter (DM) yield can be determined (Schut & Ketelaars,

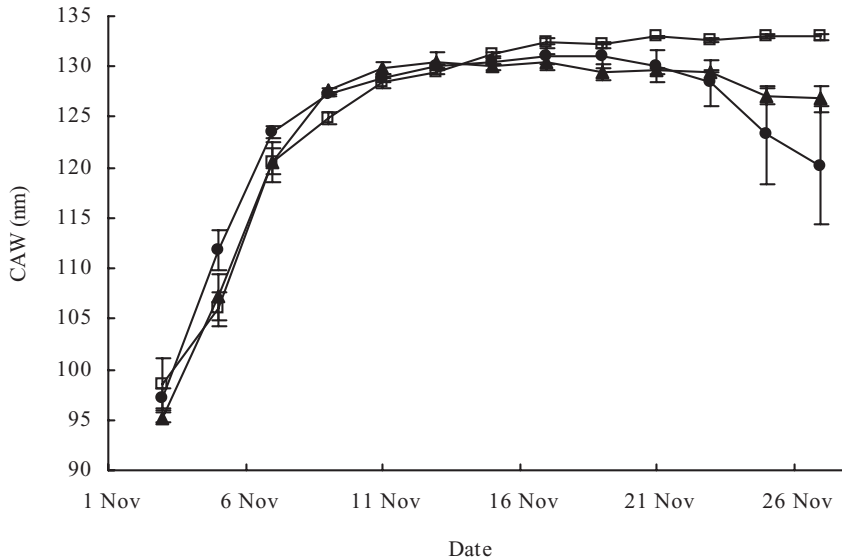


Figure 6. Development of chlorophyll-dominated absorption width (CAW) for control swards (□), drought-stressed swards with high N supply (●) and drought-stressed swards with low N supply (▲). Error bars indicate standard error of means.

2003a). Spatial standard deviation of GC (GC-SSD) slightly increased under drought stress, whereas GC-SSD of control swards decreased towards harvest. The spatial standard deviation of logarithmically transformed GC-values (TGC-SSD) just before harvest was not significantly different from the control. Schut & Ketelaars (2003b) found that at GC-values between 30 and 40%, GC-SSD of deteriorated swards ranged from 12.6 to 15.0% and TGC-SSD ranged from 0.72 to 0.85. Drought-stressed swards (with similar GC-values) remained well below these values, and it is concluded that drought stress did not significantly increase sward heterogeneity.

Within a growth period, all absorption features visible in reflectance spectra between 400 and 1650 nm deepened and widened. The positions of the detected inflection points (IP) corresponded with locations of specific absorption features of carotenoids, chlorophylls and stretching and bending of O-H, C-H and N-H bonds as reported by Lichtenthaler (1987) and Curran (1989). The minor IPs detected in the visible part of the spectrum correspond with intersections with the abscissa of the second derivative found by Buschmann & Nagel (1993). The reflection curves had a small peak around 740 nm, corresponding with the location of the chlorophyll fluorescence peak (Zarco Tejada *et al.*, 2000). This resulted in a detected IP around 770 nm.

Under drought stress all absorption features became shallower and narrower again, which is in agreement with Ripple (1986), Bowman (1989), Inoue *et al.* (1993) and Penuelas & Inoue (1999). Water absorption features (with maximum absorption around 970, 1200 and 1450 nm) responded earlier to drought stress than absorption features in the visible wavelength range, agreeing with Carter (1991; 1993). In the visi-

ble wavelength range, the position of IPs near 570 nm and 623 nm responded strongest to drought stress, agreeing with Carter (1993) who found that sensitivity is largest near 584 nm. From the moment that leaf DM content of drought-stressed swards increased, the IPs near 960, 990, 1140, 1390 and 1500 nm of drought-stressed swards significantly deviated from control swards.

Moderate drought stress did not change the position of IPs in the green and red areas of the spectrum, but clearly changed the slope near the IPs, agreeing with data of Penuelas *et al.* (1994). The absorption features in visible wavelengths responded at more advanced stages of drought when GC already decreased. This is probably due to chlorophyll breakdown and decreased light absorption of chlorophyll (Carter, 1991).

Zarco Tejada *et al.* (2000) showed that chlorophyll fluorescence emission contributes to apparent reflectance spectra of leaves with distinct peaks at 690 and 740 nm. In later growth stages leaves clearly showed an additional feature on the reflection curve, with a maximum around 740 nm. In drought-stressed swards, this feature was also present but detection was difficult due to changes in the character of the underlying reflection curve. The curve in the 740–800 nm range is nearly flat for control swards but increasing for drought-stressed swards. Carter (1991) also found flat reflection curves in this range for fresh leaves, but increasing reflection with wavelength for dehydrated and re-hydrated leaves.

The position of the IPs around 485, 624 and 705 nm also responded to the N supply level. The shift of IPs positions in the visible wavelength range during growth and under drought stress was not as strong for low N supply as for high N supply. The gradients at the IPs around 485, 517, 570, 624, 640 nm were lower for low N supply than for high N supply. In the near infra red region there were no differences found in positions and gradients of IPs between low and high N supply.

The CAW parameter reached a maximum value of 133 nm for control swards, corresponding with the findings of Schut & Ketelaars (2003c). In grass swards under moderate N stress both GE as RE showed a reversed development during the second half of a growth period, whereas GE and RE at high N showed a stable maximum (Schut & Ketelaars, 2003b). Severe drought stress also decreased CAW, which was strongest for high N supply. The relative yield of DS-HN fits well within the relation between CAW and relative yield as found earlier for N stress, whereas relative yield of DS-LN does not (Schut & Ketelaars, 2003c).

Under drought stress, the 570 nm IP position reversed in the second half of the growth period for both low and high N in parallel with GC decrease, leaf death and chlorophyll breakdown. Drought stress accelerated the increase of the IP position near 705 nm up to harvest. Horler *et al.* (1983) also reported a shift of the IP at the red edge to longer wavelengths with leaf drying. This shift to longer wavelengths can also be found in spectra of dehydrated leaves (Penuelas *et al.*, 1993). Horler *et al.* (1983) argued that this shift might result from changes in internal leaf structure.

In remote sensing with natural light, atmospheric absorption limits the detection of changes in canopy water content. Therefore, applicability of most remotely sensed indices is limited to relative water concentrations below 80–85% (Penuelas *et al.*, 1993). In our research, the combination of an active sensor and a limited distance between detector and object allowed accurate reflection measurements in strongly

water-absorbing spectral regions. In these regions early drought stress could be detected shortly before leaf water content dropped below 80%.

In the presence of a control, drought stress can be identified by comparing GC and IP position. With measurements repeated in time, the reversed shift of the IP position can identify drought-stressed swards. The position of the IP showed a clear evolution during unstressed growth. Therefore, the growth stage should be taken into account when interpreting IP positions without a control.

The relation between the IP position near 705 and 1390 nm provided such a growth stage reference, and with this relation unstressed swards shortly after harvest can be differentiated from drought-stressed swards in a later growth stage.

References

- Bowman, W.D., 1989. The relationship between leaf water status, gas exchange, and spectral reflectance in cotton leaves. *Remote Sensing of Environment* 30: 249–255.
- Buschmann, C. & E. Nagel, 1993. In vivo spectroscopy and internal optics of leaves as basis for remote-sensing of vegetation. *International Journal of Remote Sensing* 14: 711–722.
- Carter, G.A., 1991. Primary and secondary effects of water content on the spectral reflectance of leaves. *American Journal of Botany* 78: 916–924.
- Carter, G.A., 1993. Responses of leaf spectral reflectance to plant stress. *American Journal of Botany* 80: 239–243.
- Curran, P.J., 1989. Remote sensing of foliar chemistry. *Remote Sensing of Environment* 30: 271–278.
- Fernández, S., D. Vidal, E. Simon & L. Sole Sugranes, 1994. Radiometric characteristics of *Triticum aestivum* cv. Astral under water and nitrogen stress. *International Journal of Remote Sensing* 15: 1867–1884.
- Feyaerts, F. & L. Van Gool, 2001. Multi-spectral vision system for weed detection. *Pattern Recognition Letters* 22: 667–674.
- Grashoff, C., H.F.M. Aarts, H.G. Smid, R.H.E.M. Geerts & D.M. Jansen, 2001. Effect of spatial and temporal variation in drought on sward quality of grass: the need for precision irrigation. In: S. Blackmore & G. Grenier (Eds), Third European Conference on Precision Agriculture. Agro Montpellier, Montpellier, pp. 665–670.
- Horler, D.N.H., M. Dockray & J. Barber, 1983. The red edge of plant leaf reflectance. *International Journal of Remote Sensing* 4: 273–288.
- Hunt Jr., E.R., B.N. Rock & P.S. Nobel, 1987. Measurement of leaf relative water content by infrared reflectance. *Remote Sensing of Environment* 22: 429–435.
- Inoue, Y., S. Morinaga & M. Shibayama, 1993. Non-destructive estimation of water status of intact crop leaves based on spectral reflectance measurements. *Japanese Journal of Crop Science* 62: 462–469.
- Jackson, R.D. & C.E. Ezra, 1985. Spectral response of cotton to suddenly induced water stress. *International Journal of Remote Sensing* 6: 177–185.
- Jones, M.B. & A. Lazenby, 1988. *The Grass Crop: the Physiological Basis of Production*. Chapman and Hall, London, 396 pp.
- Jones, M.B., E.L. Leafe & W. Stiles, 1980a. Water stress in field-grown perennial ryegrass. 1. Its effect on growth, canopy photosynthesis and transpiration. *Annals of Applied Biology* 96: 87–101.
- Jones, M.B., E.L. Leafe & W. Stiles, 1980b. Water stress in field-grown perennial ryegrass. 2. Its effect

- on leaf water status, stomatal resistance and leaf morphology. *Annals of Applied Biology* 96: 103–110.
- Lichtenthaler, H.K., 1987. Chlorophylls and carotenoids: pigments of photosynthetic biomembranes. In: L. Packer & R. Douce (Eds), *Methods in Enzymology*, Academic Press, New York, pp. 350–382.
- Penuelas, J., I. Filella, C. Biel, L. Serrano & R. Save, 1993. The reflectance at the 950–970 nm region as an indicator of plant water status. *International Journal of Remote Sensing* 14: 1887–1905.
- Penuelas, J., J.A. Gamon, A.L. Fredeen, J. Merino & C.B. Field, 1994. Reflectance indices associated with physiological changes in nitrogen- and water-limited sunflower leaves. *Remote Sensing of Environment* 48: 135–146.
- Penuelas, J. & Y. Inoue, 1999. Reflectance indices indicative of changes in water and pigment contents of peanut and wheat leaves. *Photosynthetica* 36: 355–360.
- Railyan, V.Y. & R.M. Korobov, 1993. Red edge structure of canopy reflectance spectra of Triticale. *Remote Sensing of Environment* 46: 173–182.
- Ripple, W.J., 1986. Spectral reflectance relationships to leaf water stress. *Photogrammetric Engineering and Remote Sensing* 52: 1669–1675.
- Schut, A.G.T. & J.J.M.H. Ketelaars, 2003a. Monitoring grass swards using imaging spectroscopy. *Grass and Forage Science*. (In press)
- Schut, A.G.T. & J.J.M.H. Ketelaars, 2003b. Assessment of seasonal dry matter yield and grass sward quality with imaging spectroscopy. *Grass and Forage Science*. (In press)
- Schut, A.G.T. & J.J.M.H. Ketelaars, 2003c. Imaging spectroscopy for early detection of nitrogen deficiency in grass swards. *NJAS – Wageningen Journal of Life Sciences* 51. (This issue)
- Schut, A.G.T., J.J.M.H. Ketelaars, J. Meuleman, J.G. Kornet & C. Lokhorst, 2002. Novel imaging spectroscopy for grass sward characterisation. *Biosystems Engineering* 82: 131–141.
- Silverman, B.W., 1985. Some aspects of spline smoothing approach to non-parametric regression curve fitting. *Journal of the Royal Statistical Society B* 47: 1–22.
- Thomas, H., 1991. Accumulation and consumption of solutes in swards of *Lolium perenne* during drought and after rewatering. *New Phytologist* 118: 35–48.
- Van Loo, E.N., 1992. Tillering, leaf expansion and growth of plants of two cultivars of perennial ryegrass grown using hydroponics at two water potentials. *Annals of Botany* 70: 511–518.
- Zarco Tejada, P.J., J.R. Miller, G.H. Mohammed & T.L. Noland, 2000. Chlorophyll fluorescence effects on vegetation apparent reflectance: I. Leaf-level measurements and model simulation. *Remote Sensing of Environment* 74: 582–595.

Appendix

List of abbreviations

BE	blue edge
CAW	chlorophyll-dominated absorption width
Co	control
DM	dry matter
DS-HN	drought stressed with high N supply
DS-LN	drought stressed with low N supply
GC	ground cover
GCG	grass ground cover
GC _{IL}	image line ground cover
GCS	ground cover specular class
GC-SSD	spatial standard deviation of GC
GE	green edge
IC	reflection intensity class
IL	image line
IP	inflection point
IRI	index of reflection intensity
LAI	leaf area index
MICS	normalized spectra for each IC
MSS	mean sward reflection spectra
N	nitrogen
NIR	near infra red
RE	red edge
TGC	logistically transformed value of GC
TGC _{IL}	logistically transformed value of GC _{IL}
TGC-SSD	spatial standard deviation of TGC

